Structural and Conformational Studies of the Heparan Sulfate Mimetic PI-88

Stefano Elli,[1] Eduardo Stancanelli, [1] Paul N. Handley,[2,3] Anthony Carroll,[4,5] Elena Urso,[1] Marco Guerrini,[1] and Vito Ferro[2,6*]

[1]Istituto Scientifico di Chimica e Biochimica "G. Ronzoni", Milan 20133, Italy; [2]Progen Pharmaceuticals Ltd, Darra, Queensland 4076, Australia; [3]Current address: Zucero Therapeutics Pty Ltd, Darra, Qld 4076, Australia; [4]Griffith Research Institute for Drug Discovery, Griffith University, Nathan, Qld 4111, Australia; [5]Current address: School of Environment and Science, Griffith University Gold Coast Campus, Qld 4222, Australia; [6]Current address: School of Chemistry and Molecular Biosciences, The University of Queensland, Brisbane, Qld 4072, Australia

Running title: NMR and MD simulation studies of PI-88

Supplementary Data are included as follows:

1) ^{1}H NMR spectra for compounds **1**, **3**, **5**, **7**, **11** and **13**
2) Partial HSQC spectra for compounds **1**, **6** and **7**
3) LC-FTMS spectrum for compound **1**
4) Tables of ^{1}H and ^{13}C NMR chemical shift data for compounds **3**, **5**, **7**, **11** and **13**

Keywords: conformational analysis/ heparan sulfate mimetics/ NMR spectroscopy/ MD simulations/ PI-88

*To whom correspondence should be addressed. School of Chemistry and Molecular Biosciences, The University of Queensland, Brisbane, Qld 4072, Australia Tel.: +617 33469598; e-mail: v.ferro@uq.edu.au

Abstract

The heparan sulfate mimetic PI-88 is a complex mixture of sulfated oligosaccharides with anti-metastatic and anti-angiogenic activity due to its potent inhibition of heparanase and heparan sulfate-dependent angiogenic growth factors. It was recently in Phase III clinical trials for post-resection hepatocellular carcinoma. The major oligosaccharide constituents of PI-88 were prepared for the first time by sulfonation of individually purified phosphorylated oligosaccharides isolated from the PI-88 precursor. PI-88 and its components were subjected to detailed 1D and 2D NMR spectroscopic analysis. The spectra of the individual components greatly assisted the assignment of minor resonances in the ^{1}H NMR spectrum of PI-88. The data also showed that the majority of the oligosaccharides in PI-88 are fully sulfated and that undersulfated species present are largely due to anomeric desulfation. The solution conformation of the phosphomannopentaose sulfate (major component) of PI-88 was then determined by a combination of molecular dynamics simulations and NOE measurements which may provide insights into its binding interactions with target proteins.

Introduction

The heparan sulfate (HS) mimetic PI-88 (also known as muparfostat or "phosphomannopentaose sulfate") (Parish, C.R., et al. 1999) is an inhibitor of angiogenesis, tumour growth and metastasis that has been in clinical development for the past two decades in various cancer indications (Basche, M., et al. 2006, Chow, L.Q., et al. 2008, Khasraw, M., et al. 2010, Kudchadkar, R., et al. 2008, Lewis, K.D., et al. 2008). Most recently, PI-88 was evaluated in an international, multi-centre Phase III clinical trial as an adjuvant therapy for post-resection hepatocellular carcinoma (Liao, B.Y., et al. 2016, Liu, C.J., et al. 2014, Liu, C.J., et al. 2009). PI-88 is a potent inhibitor of angiogenesis (Ferro, V., et al. 2007, Joyce, J.A., et al. 2005, Parish, C.R., Freeman, C., et al. 1999). This activity is mediated through inhibition of heparanase (Parish, C.R., Freeman, C., et al. 1999), an endo-β-glucuronidase that plays a key role in both metastasis and angiogenesis (Pisano, C., et al. 2014, Sanderson, R.D., et al. 2017, Vlodavsky, I., et al. 2012, Vlodavsky, I., et al. 2016), and more directly via blocking the interactions of angiogenic growth factors, such as FGF-1, FGF-2 and VEGF, and their receptors with HS (Fairweather, J.K., et al. 2008, Francis, D.J., et al. 2003, Parish, C.R., Freeman, C., et al. 1999).

PI-88 (**1**, Fig. 1) is a complex mixture of monophosphorylated, polysulfated mannose oligosaccharides. It is prepared by the exhaustive sulfonation of the oligosaccharide phosphate fraction (OPF) obtained following mild acid-catalysed hydrolysis of the extracellular phosphomannan produced by the yeast *Pichia holstii* NRRL Y-2448 (Ferro, V., et al. 2001, Yu, G., et al. 2002). This mixture is primarily composed of phosphorylated $\alpha(1\rightarrow3)/\alpha(1\rightarrow2)$-linked penta- and tetrasaccharides, which together account for approximately 90% of the total oligosaccharide content, with the remaining

10% comprised of phosphorylated di-, tri- and hexasaccharides (Ferro, V., et al. 2002, Parolis, L.A., et al. 1998).

Recently, the OPF was successfully separated for the first time by preparative ion exchange chromatography and the major oligosaccharides were isolated and characterized by NMR spectroscopy and MS (Handley, P.N., Carroll, A, et al. 2017). The presence of the previously reported oligosaccharide phosphates **2**, **4**, **6** and **8**, which possess α(1→3)-linked mannoses with a terminal α(1→2)-linked residue, was confirmed with **4** and **6** as the major components (Fig. 1). The presence of the all-α(1→3)-linked isomers **12**, **14**, and **16** resulting from hydrolytic cleavage of higher oligosaccharides, and present in amounts that vary inversely with oligosaccharide chain length, was also confirmed. It was also shown that the only disaccharide phosphate present is the α(1→3)-linked **10** (Handley, P.N., Carroll, A., et al. 2017). Given that the OPF is exhaustively sulfonated to produce PI-88, it was proposed that the structure of PI-88 is best represented by structure **1** (Fig. 1) as this more accurately reflects its composition. Herein we describe the preparation of the individual components of PI-88 from the successfully separated OPF oligosaccharides and their detailed structural characterization by NMR spectroscopy, which when combined with detailed NMR spectroscopic analysis of PI-88 itself, allowed for the assignment of many minor resonances in the ^{1}H NMR spectrum of PI-88 and provided new insights into its composition and level of sulfation. In addition, a detailed conformational analysis of the phosphomannopentaose sulfate, the major component of PI-88, was carried out by combining data from NOESY spectra with molecular dynamics simulations.

Results and Discussion

Samples of the purified OPF oligosaccharides (Handley, P.N., Carroll, A., et al. 2017) were individually sulfonated by treatment with excess sulfur trioxide pyridine

complex to yield the corresponding PI-88 component oligosaccharides following purification by size exclusion chromatography (Bio-Gel P2). The purity was determined to be ≥95% by capillary electrophoresis. After sulfonation, the corresponding sulfated pentasaccharide fraction was examined in D_2O at both 500 and 600 MHz using one- and two-dimensional NMR techniques and the ^{1}H and ^{13}C NMR chemical shifts were fully assigned (see Table S1, Supplementary Data) using the HSQC, HMBC, COSY and TOCSY pulse sequences (Fig. S1, S2 and S4). Ambiguous assignments, such as the inter-ring connectivity were resolved by NOESY (Fig. S3) and HMBC experiments (Fig S4). These data clearly established the fully sulfated α-anomer of pentasaccharide **7** as the major component, with ~10% of the β-anomer also present (integration of corresponding anomeric signals of the proton spectrum. Data not shown).

A significant downfield shift was generally observed in the ^{1}H NMR spectrum for the resonances of protons geminal to hydroxy groups upon sulfation, with no signals between 3.6 and 4 ppm, indicative of full *O*-sulfation (Fig. 2). Similarly, the resonances of carbon atoms attached to sulfo groups in **7** were shifted downfield relative to the corresponding resonances in the non-sulfated precursor **6** (Fig. 2 and S5). Carbon atoms involved in glycosidic linkages were observed to resonate at slightly higher field upon sulfation (<3 ppm for ^{13}C). The average resonances of the hydroxylated carbon atoms shifted 6.0 ppm downfield upon sulfation, and the corresponding shifts in the proton spectrum were 0.73 ppm. The small shift for C6 of the non-reducing end mannose residue is consistent with the presence of a phosphate group in this position.

The shapes of the signals for the anomeric protons of the reducing end residue (A) in the NMR spectra of **7** are noteworthy. The larger line widths (e.g., see Fig. S1, A1-α) are probably due to shorter relaxation times (T2) with respect to the other anomeric

protons. The presence of a very high degree of sulfation influences the internal mobility of the molecule with the introduction of local rigidity due to steric hindrance and/or inter-residue interactions, as discussed in the MD simulations section (*vide infra*).

The major components of the sulfated tetra-, tri-, and disaccharide fractions were similarly assigned as described above (Tables S2-S5 and Fig. S6-S8). The anomeric ratios observed in the non-sulfated oligosaccharide precursors (Handley, P.N., Carroll, A., et al. 2017) were roughly preserved upon sulfation. Although the minor β-anomers (Aβ ring) were fully assigned in the case of all-(1→3)-linked structures **11** and **13**, in the case of oligosaccharides **3**, **5** and **7** with a terminal (1→2)-linked residue, the minor β-anomers were much less abundant. The NMR spectral resonances of the latter compounds were insufficiently resolved for full assignment; partial assignments were made as illustrated for the pentasaccharide **7** where the protons nearest the reducing-end residue could be determined. Confirmation of the β-configuration at the anomeric centre was available from the unusual downfield shift of the anomeric proton of residue (B) (labelled peak H1 B-(Aβ) in Fig. S9) upon NMR analysis. This proton resonates at a chemical shift of δ_H 5.76, which is at unusually low field for a non-sulfated anomeric centre. Fig. S9 also shows the peak assigned to proton H-1 Aβ at the sulfated anomeric centre. The chemical shift of peak H1 B-(Aβ) can be rationalised as the result of deshielding by a through-space interaction with at least three sulfate groups that are linked to C2 of residue B, and also to C1 and C3 of residue A. (Martin, N.H., et al. 2006). Further confirmation of the assignment of peaks H1 B-(Aβ) and H1 Aβ was available from the NOESY spectrum, as the expected cross-peaks were observed between both protons and H2 Aβ (Fig. S2). The NMR spectra of PI-88 and of the sulfated tetrasaccharide **5** exhibited a very similar pattern of resonances assigned to α- and β-anomers (Fig. S1).

NMR spectroscopic characterisation of the sulfated trisaccharide fraction confirmed that the major components were the α- and β-anomers of compound **13**, and the α- and β-anomers of compound **3**, in the ratio of 5:2:3:0.2. The ^{1}H NMR spectra of the first three compounds were fully assigned (see Tables S3 and S4). The reducing end anomeric proton of the α-anomer of compound **13** is very distinctive, resonating at δ_H 6.02, the lowest field of any anomeric proton observed in this study. Thus, the small group of signals around 6 ppm in the ^{1}H NMR spectrum of PI-88 are characteristic of the minor all-(1→3)-linked isomers (Fig. S1, S2 and S10). The reducing end anomeric proton of the β-anomer of compound **13** is obscured by the strong signals at approximately δ_H 5.5.

As discussed above, the NMR chemical shifts of hydroxylated carbon atoms and their attached protons were significantly increased upon sulfation of each OPF fraction. As this shift was observed for all 16 free hydroxyl groups in pentasaccharide **6**, it was concluded that the major component in the pentasaccharide fraction was the completely per-*O*-sulfated pentasaccharide **7**, with the α-configuration at the anomeric centre. The presence of a small amount (~10%) of the corresponding β-anomer was also noted. Similarly, the major components in the sulfated tetra-, tri-, and disaccharide fractions were shown to be fully sulfated, with anomeric ratios consistent with those observed for the unsulfated precursors. This is well illustrated by superimposition of the HSQC spectra of compound **7** and its precursor **6** (Fig. 2). As the NMR spectra of PI-88 were very similar to those of pentasaccharide **7**, it was concluded that the major components in PI-88 were also fully per-*O*-sulfated (Fig. S5). This is consistent with the C:S ratio data from elemental analysis (Cochran, S., et al. 2003) and LC-ESI-FTMS. The LC-MS profile shows a main peak corresponding to the mass of compound **7** determined as Mw = 2189.6 Dalton, and minor peaks attributed to the mono-desulfated pentasaccharide and shorter oligomers from di- to tetrasaccharides (Fig. S11). The full scan mass spectra corresponding to each

chromatographic peak of the recorded LC-MS profile is shown in Supp. Fig. S12, while the expanded mass spectra of the parent ions and comparison between theoretical and experimental isotopic patterns is in Supp. Fig. S13.

The original PI-88 sample in this study was split into two portions, with one sample examined in Australia at 600 MHz and the other sent to Italy for independent analysis initially at 500 MHz. Although the PI-88 samples were identical, the delay in sample measurement due to the long trip to Italy presumably resulted in more opportunity for decomposition as the 500 MHz spectrum exhibited significant differences compared with that at 600 MHz; the anomeric proton signal of the reducing-end mannose residue was slightly reduced in intensity, and new resonances appeared around 5.42 ppm and 5.56 ppm. The intensities of these signals further increased after two days from NMR tube preparation (Fig. 3). These NMR spectral features are consistent with slight decomposition by anomeric desulfation. This was confirmed by superimposition of the HSQC spectra of PI-88 and unsulfated pentasaccharide **6** (Fig. S5). The nascent anomeric resonance corresponding to the reducing end of compound **7**, correlates to that for the reducing-end anomeric resonance of pentasaccharide **6**, indicating that they are in very similar chemical environments, i.e., both are unsulfated. The amount of anomeric desulfation in the sample was estimated to be 14%, calculated by comparison of the cross-peak volume of its signal with that of its sulfated counterpart. The second peak at δ_H 5.56 was assigned to mannose residue B linked to the reducing mannose desulfated at the anomeric position. Again, this is best illustrated by the HSQC spectrum (Fig. S1) where small resonances at ~ δ_H/ δ_C 5.4/95 and ~ δ_H/ δ_C 5.55/101 corresponding to the anomeric proton of residues A and B of the desulfated product are indicated by the arrow.

A detailed conformational analysis of PI-88 in solution was also accomplished. A fresh sample of PI-88 was analysed by NMR spectroscopy at 600 MHz and a complete assignment of the chemical shifts was carried out via COSY, TOCSY, HSQC, HMBC and NOESY experiments. The $^{1}H/^{13}C$ chemical shifts, summarized in Table 1, are largely in agreement with those obtained for the pentasaccharide **7,** despite the systematic shift of the carbon resonances (minor for proton), due to the use of a different reference standard. The inter-residue NOEs not only confirmed inter-residue connectivities but also provided information on the geometry of the glycosidic linkages. To reduce spin-diffusion effects, the inter-glycosidic proton-proton distances were estimated by two-spin approximation at short mixing time (200 ms). The H1-H2 distance of internal mannose residues (2.53Å) was used as a reference distance.

Cross-peaks between H1 and H3 and between H2 and H5 were observed across each glycosidic linkage in going from residue E to B; while the glycosidic linkage involving residues B and A showed H1B-H2A, H1B-H1A and H1A-H5B NOE correlations (See Fig. S2 and S3). The corresponding estimated distances are reported in the second column of Table 2. This set of NOE cross-peaks observed between E to A residues of PI-88, agrees with a $^{4}C_{1}$ chair conformation of all mannose residues, similarly to that previously described for unsulfated Man-α(1→3)-Man oligosaccharides (Almond et al. 2001). Unfortunately, the heterogeneity of the mixture and the consequent signal broadening does not allow the determination of selected three bond $^{3}J_{HH}$ coupling constants, to directly support the conformation of these residues.

MD simulations

The conformational characterization of the polysulfated pentasaccharide and its non-sulfated precursor (compounds **7** and **6,** respectively), was carried out by a succession of

eleven MD simulation steps with temperature increasing from 300 K (1ststep) to a maximum value of 400 K (6thstep) and then decreasing back to a final value of 300 K in the final (11th) step, with this last step further considered for the glycosidic backbone optimization. The MD simulation procedure was then terminated by a simulated annealing process, in which the temperature was progressively reduced from 300 K to 20 K, until a final energy minimization was applied to generate the final structures to be optimized in their glycosidic backbone, before their comparison with the PI-88 measured NOE restraints. The length of each MD simulation step was set to 20 ns, while the duration of the whole MD simulation sequence was 220 ns (see Material and Methods). This variable temperature approach was chosen considering the high conformational stiffness of the glycosidic linkages of these poly-sulfated oligosaccharides and should allow a more efficient exploration of their conformational space compared with a constant temperature MD simulation of similar length. Conformational transitions of each Man residue, set initially in the $^{4}C_{1}$ chair for both sulfated and non-sulfated pentasaccharides, was monitored by the intra-residue distance H3-H5. Even if each residue maintains its initial $^{4}C_{1}$ chair for the whole MD simulation, the H3-H5 distance calculated in the final MD simulation sampling (step 11th), suggest a significant distorsion of the $^{4}C_{1}$ chair in the polysulfated pentasaccharide (compound **7**), in comparison with the less crowded non-sulfated precursor (compound **6**). In fact, the average H3-H5 distance is significantly greater in compound **7** (> 2.6 Å) than in compound **6** in all the rings except in residue B. (Supp. Tab. S6). The ideal case of a cyclohexane chair conformation shows equal inter-proton distances: H1-H3, H1-H5 and H3-H5 approaching the 2.6 Å value. The optimization of the glycosidic backbone conformations of compound **7** and **6**, obtained at the end of the simulated annealing, involve the determination of the most populated states on the MD simulation trajectories of the last step (11th) in the previously cited multi-step

procedure. Ramachandran plots of ϕ/ψ dihedrals were drawn combining a 2D histogram binning and a coloured density maps (Fig. 4), (see Materials and Methods). The estimated glycosidic dihedral angles with an uncertainty of approximately ± 10° are reported in Table 3. The efficiency in the glycosidic backbone conformational sampling is verified on the stiffest molecule (compound **7**) comparing the 2D histogram binning analysis on the 1st, the 6th, and the 11th MD simulation steps; the obtained Ramachandran plots are reported in the first, second and third column respectively of Supp. Fig. S14. Fig. S14 shows significant glycosidic linkage conformational changes in going from the early to the later stages of the multi-step MD simulation, showing how the stiffest polysulfated phosphomannopentose appears not stuck in its initial conformation, but visiting a growing number of states as the temperature increases, improving the possibility to populate the most favoured conformers. Figure 4 shows for both pentasaccharides a comparable ϕ/ψ distribution at central linkages (D-C and C-B), while the non-reducing and reducing (E-D, B-A) glycosidic linkages significantly differ from the previous. This result is expected considering that the last two glycosidic junctions include the two terminal residues, and B-A has (1→2) instead of (1→3) connectivity. Figure 4 clearly shows the decrease in dihedral angle conformational freedom in going from a non-sulfated pentasaccharide to a polysulfated analogue, the latter characterized by a stiffer glycan backbone (compare the right and left columns in Fig. 4). In fact, all glycosidic linkages show a significantly narrower ϕ/ψ distribution and higher gradient of colours (from the reds to the blue shadows) in the polysulfated pentasaccharide (compound **7**). The E-D glycosidic junction of compond **6** shows a wider ϕ/ψ conformational space, possibly split in three different regions approximately centred in: -30/50, -40/20, -40/-20, considering the continuity of the yellow/red shadows of the coloured bins (Fig. 4, E-D panel, right and left columns). A deeper conformational analysis on this glycosidic bond is required to confirm these

potential energy minimae. The predicted linear conformation and selected inter-glycosidic distances of compound **7** and **6** are shown in Figure 5 right and left respectively, both molecules appear linear, even if compound **7** shows the stiffest conformation for the highest crowding. The selected inter-glycosidic distances for the polysulfated pentasaccharide are then compared in Table 2 and found qualitatively in accord with the corresponding distances estimated by NOEs.

Conclusions

The major oligosaccharide constituents of PI-88 were prepared by sulfonation of individual purified phosphorylated oligosaccharides isolated from the PI-88 precursor and subjected to detailed 1D and 2D NMR spectroscopic analysis. The spectra of the individual components greatly assisted the assignment of minor resonances in the ^{1}H NMR spectrum of PI-88. The data also showed that most of the oligosaccharides in PI-88 are fully sulfated and that undersulfated species present are largely due to anomeric desulfation. These studies then allowed the full assignment of the ^{1}H and ^{13}C NMR spectra of PI-88.

For the first time, the conformational characterization of the phosphomannopentaose sulfate with Man-α(1→3)-Man connectivities and terminated at its reducing end by the Man-α(1→2)-Man glycosidic linkage is reported and compared with the corresponding unsulfated precursor. The NOE signals determined from the complex mixture, in which pentasaccharide **7** is prevalent, show correlations across each glycosidic linkage, involving different pairs of protons between internal and reducing end residues. The $^{4}C_{1}$ chair conformation of each Man residue, already described for unsulfated Man-α(1→3)-Man oligosaccharides (Almond, A., et al. 2001), appears to be unaffected by sulfation as supported by the series of inter-glycosidic NOEs proton pair correlations observed, even if a weak distorsion of the $^{4}C_{1}$ conformation appear correlated to the high degree of sulfation of compound **7**, in comparison with the corresponding un-sulfated precursor **6**. MD simulations in implicit solvent and a 2D histogram binning procedure allowed the sampling and qualitative prediction of the conformation of Man-α(1→3)-Man and the reducing end Man-α(1→2)-Man glycosidic junctions (Ramachandran plots) in both polysulfated and unsulfated pentasaccharides. In particular,

the glycosidic conformation predicted by the ϕ/ψ 2D density maps of the former compound qualitatively match the inter-glycosidic NOE restraints. Comparison of the Ramachandran plots of polysulfated and unsulfated pentasaccharides suggests a decrease in conformational freedom (increase in backbone stiffness) upon sulfation at each glycosidic junction. These results predict a linear and rigid backbone conformation for the longest, and most abundant polysulfated oligosaccharides in the PI-88 mixture, and a similar but less stiff conformation for their corresponding un-sulfated precursors, providing useful insights to understand the binding interactions of PI-88 with target proteins.

Materials and Methods

General Methods

Solvents used were HPLC grade unless stated otherwise. CE analyses were performed in reverse polarity mode on an Agilent CE System using 10 mM 5-sulfosalicylic acid, pH 3, as the background electrolyte and detection by indirect UV absorbance at 214 nm, as previously described (Yu, G., Gunay, N.S., et al. 2002). Size-exclusion chromatography was performed over Bio-Gel P2 eluting with 0.1 M NH_4HCO_3 supplied by a Pharmacia LKB Pump P-500 at 196 mL/h, and 20 mL fractions were collected using a Pharmacia LKB Frac-200 fraction collector. Fractions were quickly checked using a combination of the H_2SO_4 char test and metachromatic staining with 1,9-dimethyl methylene blue, and those containing product were diluted for analysis by CE. Fractions judged to contain a significant amount of salt-free product were combined and lyophilized, then redissolved in HPLC water and lyophilized again.

Sulfonation of the pentasaccharide fraction

A mixture of pentasaccharide **6** (980 mg, 1.04 mmol, purity 94.4%) and sulfur trioxide pyridine complex (9.0 g, 56 eq., ~3 eq. per hydroxyl group) in anhydrous DMF (25 mL) was stirred for 45 h. The DMF solvent was decanted, and the gummy precipitate was washed briefly with anhydrous EtOH (2 mL) and then dissolved in water (5 mL). The resulting strongly acidic (pH 1.4) solution was basified to pH 9.3 by the addition of 2M NaOH solution (10.2 mL). Free pyridine was removed by washing with DCM (5 × 5 mL). The pale brown aqueous layer was decolorized by passage through a Waters Sep-Pak Vac 20cc C18-5g solid-phase extraction cartridge, pre-conditioned by wetting with MeOH, then washing with water:MeOH (1:1→9:1→99:1). The oligosaccharide was loaded as a solution in 99:1 water:MeOH and the cartridge was washed with 99:1 water:MeOH (60 mL) until the eluate tested negative for the presence of carbohydrates (H_2SO_4 char). The appropriate fractions were combined and evaporated to dryness. The resulting glassy solid was desalted by size exclusion chromatography to give the sulfated pentasaccharide **7** (1.02 g, 37.9%) as a white solid. ^{1}H and ^{13}C NMR chemical shift data are presented in Table S1.

Sulfonation of the tetrasaccharide fraction

The tetrasaccharide **4** (300 mg, 0.38 mmol) was sulfonated as described above for the pentasaccharide **6** to give the sulfated tetrasaccharide **5** (447 mg, 55 %) as an off-white solid. ^{1}H and ^{13}C NMR chemical shift data are presented in Table S2.

Sulfonation of the trisaccharide fraction

The trisaccharide fraction of the OPF (297 mg, 0.48 mmol) was sulfonated as described above to give the sulfated trisaccharide fraction containing a mixture of compounds **13** and **3** (497 mg, 63 %) as an off-white solid. ^{31}P NMR (162 MHz, D_2O): δ 3.94. ^{1}H and ^{13}C NMR chemical shift data are presented in Tables S3 and S4.

Sulfonation of the disaccharide fraction

The disaccharide **10** (100 mg, 0.22 mmol) was sulfonated as described above to give the sulfated disaccharide **11** (150 mg, 58 %) as an off-white solid. ^{31}P NMR (162 MHz, D_2O): δ 3.88. ^{1}H and ^{13}C NMR chemical shift data are presented in Table S5.

Mass spectrometry

LC-MS analysis was performed on a HPLC 1100 (Agilent) coupled to a 7.0 T Fourier transform ion cyclotron resonance (FTICR) mass spectrometer equipped with electrospray (ESI) source (Solarix, Bruker). The ion pair reversed phase (IP RP) liquid chromatography separation was conducted on a Kinetex C18 column (2.1 × 100 mm, 2.6 µm particle size, Phenomenex, Aschaffenburg, Germany) using dibutylamine for ion paring. A volume of 3 µL of the sample solution prepared at the concentration of 0.2 mg/mL was introduced via an autosampler; the separation was carried out at 30 °C by running the mobile phases A (dibutylamine 10 mM, acetic acid 10 mM in water) and B (dibutylamine 10 mM, acetic acid 10 mM in methanol) at 0.1 mL/min according to the following gradient scheme: isocratic step at 25% B for 2 min, followed by a fast linear gradient to 60% B in 3 min and a second slower gradient from 60% to 95% B in 30 min; then, the column was held at 95% B for 5 min and re-equilibrated to the initial conditions. High resolution full mass scan spectra were recorded in negative polarity in the mass range from 200 to 3000 using the following ESI source parameters: capillary voltage: +3200 V, nitrogen gas used as nebulizer and heater gases was set at 1.0 bar and 3.7 L/min, respectively. Mass calibration was performed by using sodium formate solution (water–isopropanol 1:1 v/v solution containing HCOOH 0.2% and NaOH 5 $\times 10^{-3}$ N).

NMR Spectroscopy

NMR data at 500 and 600 MHz were recorded in D_2O; chemical shifts of the isolated oligosaccharides are reported in ppm relative to D_2O at 4.80 for ^{1}H and externally referenced to TMS 0.0 for ^{13}C at 30 ºC. Chemical shifts of PI-88 are reported in ppm externally referenced to TSP 0.0 for ^{13}C and ^{1}H at 30 ºC. ^{1}H resonances for oligosaccharides were fully assigned using the HSQC and COSY pulse sequences, and the inter-ring connectivity was established using HMBC correlations. Oligosaccharide residues are indicated with consecutive letters from the reducing end. Proton spectra were recorded with water presaturation with a recycle delay of 12 s and 16 scans. HSQC (heteronuclear single quantum coherence) and HMBC (heteronuclear multiple bond correlation) experiments were performed in phase sensitivity enhanced pure-absorption mode using 16 dummy scans, 16 and 32 scans, respectively, with decoupling during acquisition period and 2.5 s of relaxation delay. The matrix size of 2048 × 320 data points was increased to 4096 × 1024 by linear prediction and zero filling. 2D homonuclear correlation COSY and TOCSY experiments were obtained in phase sensitivity mode using 8 scans with water presaturation during acquisition. In TOCSY experiments isotropic mixing was performed applying a MLEV pulse train of 100 ms. NOESY experiments were obtained with a total of 16 scans, a mixing time of 150 ms and a recycle delay of 5.5 s. All homonuclear correlation experiments were acquired with a matrix size of 1048 × 320 data points with zero filling in F1 (2048 × 1024) before Fourier transformation.

NOESY analysis

The estimation of the inter-glycosidic distances was done by correlating the ratio between the % of NOEs generated by a selected Hx-Hy pair across the glycosidic bond, whose distance is unknown, and the % of NOEs of the reference pair H1-H2, that belong to a Man residue whose distance is 2.53 Å. (see eq. 1).

$$\left.\frac{\%NOE(H-Hx)}{\%NOE(H1-H2)}\right|_{Tmix} = \left(\frac{r(H1-H2)}{r(H-Hx)}\right)^6 \quad (1)$$

In eq. 1 the suffix "Tmix" indicates that only the NOE % measured at the lowest mixing time is considered. Due to the large line widths of the anomeric signals of residue A and B, NOE intensities were referenced to one third of H1 of E+C+D diagonal peak volumes.

MD simulations

Models of polysulfated and nonsulfated pentasaccharides (compounds **7** and **6**, respectively) were built using Maestro/Macromodel 9.8 software, where the Man residues were set initially in the $^4C_1$ conformation, and the connectivity between residues is Man-α(1→3)-Man, except for the glycosidic junction at the reducing end, whose connectivity is Man-α(1→2)-Man (see NMR section and Almond *et al.* 2001). For Molecular Mechanics and MD simulations the Amber* force field as implemented in Maestro/Macromodel 9.8 was used, which include Homan's parameters and atom types for pyranose (Homans S. W., et al. 1990). The non-bonded cut-offs were set to 20.0, 8.0 and 4.0 Å for electrostatic, van der Waals and hydrogen bond interactions, respectively. The solvent description involved the Generalized Born Implicit Solvent method as implemented in Macromodel. The two glycan models after building were energy minimized (bmin) setting the Max number of steps = 10 K, and Energy Gradient Threshold = 10^{-3} KJ mol^{-1}Å^{-1}. The energy minimization algorithm chosen was the PRCG (Polak-Ribiere Conjugate Gradient). The two glycan models were then submitted to a multi-step sequence of eleven MD simulation runs with temperature progressively increasing from 300 K (1st step) to the highest temperature value of 400 K (6th step) using steps of 20 K, decreasing again to the final value of 300 K, this last (11th step) being the production step, in which the glycosidic ϕ/ψ

distribution were determined using a 2D histogram binning approach as further explained. The time length of each fixed temperature MD run was 20 ns for a whole duration of 220 ns. The MD simulations were terminated by a simulated annealing, in which the temperature is progressively reduced (using steps of 100 ps length and ΔT = 20 K) from T = 300 K to 20 K, before to apply a final energy minimization; the obtained geometries of compound **7** and **6** were optimized in their backbone using the glycosidic dihedral angles determined by 2D histogram binning applied on the final stage (11^{th} step) of the multi-step MD simulation. The conformational sampling of the two pentasaccharides was analysed using Ramanchandran plots for each glycosidic linkage; each plot was built using a 2D histogram binning approach, where a coloured density map allowed the localization of the most populated ϕ/ψ states with an accuracy of ±10°, that corresponds to approximately half of the smallest unit of a 2D histogram binning grid. To evaluate the efficiency of the multi-step MD simulation approach on the conformational sampling of compound **7,** the 2D histogram binning analysis is applied also on the 1^{st} and 6^{th} MD step and compared to the production step (11^{th}). (See Supp. Fig. S14 first, second and third columns respectively).

The dihedral angle states ϕ/ψ are reported in Table 3 for both compound **7** and **6**. The predicted conformation for both compounds are reported in Figure 5, with selected inter-glycosidic distances, while Table 2 includes the selected inter-glycosidic distances of compound **7** to compare with the corresponding values estimated from the NOEs signals. The R-statistical software (hexbin package), was used to generate the 2D histograms of the Ramachandran plots (Azzalini, A., et al. 2012).

Funding

This work was partially supported by the Australian Research Council [DP170104431 to V.F.]

Acknowldegements

We gratefully acknowledge Cai Ping Li for the CE analyses.

References

Almond A, Bunkenborg J, Franch T, Gotfredsen CH, Duus JØ. 2001. Comparison of aqueous molecular dynamics with NMR relaxation and residual dipolar couplings favors internal motion in a mannose oligosaccharide. *J. Am. Chem. Soc.*, 123:4792-4802.

Azzalini A, Menardi G, Rosolin T. 2012. R package pdfCluster: Cluster analysis via nonparametric density estimation, version 1.0-0. Universitá di Padova, Padua, Italy.

Basche M, Gustafson DL, Holden SN, O'Bryant CL, Gore L, Witta S, Schultz MK, Morrow M, Levin A, Creese BR, *et al.* 2006. A phase I biological and pharmacologic study of the heparanase inhibitor PI-88 in patients with advanced solid tumors. *Clin. Cancer Res.*, 12:5471-5480.

Chow LQ, Gustafson DL, O'Bryant CL, Gore L, Basche M, Holden SN, Morrow MC, Grolnic S, Creese BR, Roberts KL, *et al.* 2008. A phase I pharmacological and biological study of PI-88 and docetaxel in patients with advanced malignancies. *Cancer Chemother. Pharmacol.*, 63:65-74.

Cochran S, Li C, Fairweather JK, Kett WC, Coombe DR, Ferro V. 2003. Probing the interactions of phosphosulfomannans with angiogenic growth factors by surface plasmon resonance. *J. Med. Chem.*, 46:4601-4608.

Fairweather JK, Hammond E, Johnstone KD, Ferro V. 2008. Synthesis and heparanase inhibitory activity of sulfated mannooligosaccharides related to the antiangiogenic agent PI-88. *Bioorg. Med. Chem.*, 16:699-709.

Ferro V, Dredge K, Liu L, Hammond E, Bytheway I, Li C, Johnstone K, Karoli T, Davis K, Copeman E, *et al.* 2007. PI-88 and novel heparan sulfate mimetics inhibit angiogenesis. *Semin. Thromb. Hemost.*, 33:557-568.

Ferro V, Fewings K, Palermo MC, Li C. 2001. Large-scale preparation of the oligosaccharide phosphate fraction of Pichia holstii NRRL Y-2448 phosphomannan for use in the manufacture of PI-88. *Carbohydr. Res.*, 332:183-189.

Ferro V, Li C, Fewings K, Palermo MC, Linhardt R, Toida T. 2002. Determination of the composition of the oligosaccharide phosphate fraction of *Pichia (Hansenula) holstii* NRRL Y-2448 phosphomannan by capillary electrophoresis and HPLC. *Carbohydr. Res.*, 337:139-146.

Francis DJ, Parish CR, McGarry M, Santiago FS, Lowe HC, Brown KJ, Bingley JA, Hayward IP, Cowden WB, Campbell JH, *et al.* 2003. Blockade of vascular smooth muscle cell proliferation and intimal thickening after balloon injury by the sulfated oligosaccharide PI-88: phosphomannopentaose sulfate directly binds FGF-2, blocks cellular signaling, and inhibits proliferation. *Circ. Res.*, 92:e70-77.

Handley PN, Carroll A, Ferro V. 2017. New structural insights into the oligosaccharide phosphate fraction of *Pichia (Hansenula) holstii* NRRL Y2448 phosphomannan. *Carbohydr. Res.*, 446-447:68-75.

Homans, S. W. 1990. A molecular mechanical force field for the conformational analysis of oligosaccharides: Comparison of theoretical and crystal structures of Man-α1,3-Man-β1,4-GlcNAc. *Biochemistry* 29:9110-9118.

Joyce JA, Freeman C, Meyer-Morse N, Parish CR, Hanahan D. 2005. A functional heparan sulfate mimetic implicates both heparanase and heparan sulfate in tumor angiogenesis and invasion in a mouse model of multistage cancer. *Oncogene*, 24:4037-4051.

Khasraw M, Pavlakis N, McCowatt S, Underhill C, Begbie S, de Souza P, Boyce A, Parnis F, Lim V, Harvie R, *et al.* 2010. Multicentre phase I/II study of PI-88, a heparanase inhibitor in combination with docetaxel in patients with metastatic castrate-resistant prostate cancer. *Ann. Oncol.*, 21:1302-1307.

Kudchadkar R, Gonzalez R, Lewis KD. 2008. PI-88: a novel inhibitor of angiogenesis. *Expert Opin. Investig. Drugs*, 17:1769-1776.

Lewis KD, Robinson WA, Millward MJ, Powell A, Price TJ, Thomson DB, Walpole ET, Haydon AM, Creese BR, Roberts KL, *et al.* 2008. A phase II study of the heparanase inhibitor PI-88 in patients with advanced melanoma. *Invest. New Drugs*, 26:89-94.

Liao BY, Wang Z, Hu J, Liu WF, Shen ZZ, Zhang X, Yu L, Fan J, Zhou J. 2016. PI-88 inhibits postoperative recurrence of hepatocellular carcinoma via disrupting the surge of heparanase after liver resection. *Tumour Biol.*, 37:2987-2998.

Liu CJ, Chang J, Lee PH, Lin DY, Wu CC, Jeng LB, Lin YJ, Mok KT, Lee WC, Yeh HZ, *et al.* 2014. Adjuvant heparanase inhibitor PI-88 therapy for hepatocellular carcinoma recurrence. *World J. Gastroenterol.*, 20:11384-11393.

Liu CJ, Lee PH, Lin DY, Wu CC, Jeng LB, Lin PW, Mok KT, Lee WC, Yeh HZ, Ho MC, *et al.* 2009. Heparanase inhibitor PI-88 as adjuvant therapy for hepatocellular carcinoma after curative resection: a randomized phase II trial for safety and optimal dosage. *J. Hepatol.*, 50:958-968.

Martin NH, Loveless DM, Main KL, Pyles AK. 2006. Computation of through-space NMR shielding effects by functional groups common to peptides. *J. Mol. Graphics Modell.*, 25:1-9.

Parish CR, Freeman C, Brown KJ, Francis DJ, Cowden WB. 1999. Identification of sulfated oligosaccharide-based inhibitors of tumor growth and metastasis using novel in vitro assays for angiogenesis and heparanase activity. *Cancer Res.*, 59:3433-3441.

Parolis LA, Parolis H, Kenne L, Meldal M, Bock K. 1998. The extracellular polysaccharide of *Pichia (Hansenula) holstii* NRRL Y- 2448: the phosphorylated side chains. *Carbohydr. Res.*, 309:77-87.

Pisano C, Vlodavsky I, Ilan N, Zunino F. 2014. The potential of heparanase as a therapeutic target in cancer. *Biochem Pharmacol*, 89:12-19.

Sanderson RD, Elkin M, Rapraeger AC, Ilan N, Vlodavsky I. 2017. Heparanase regulation of cancer, autophagy and inflammation: new mechanisms and targets for therapy. *FEBS J*, 284:42-55.

Vlodavsky I, Beckhove P, Lerner I, Pisano C, Meirovitz A, Ilan N, Elkin M. 2012. Significance of heparanase in cancer and inflammation. *Cancer Microenviron.*, 5:115-132.

Vlodavsky I, Singh P, Boyango I, Gutter-Kapon L, Elkin M, Sanderson RD, Ilan N. 2016. Heparanase: From basic research to therapeutic applications in cancer and inflammation. *Drug Resist Updat*, 29:54-75.

Yu G, Gunay NS, Linhardt RJ, Toida T, Fareed J, Hoppensteadt DA, Shadid H, Ferro V, Li C, Fewings K, *et al.* 2002. Preparation and anticoagulant activity of the phosphosulfomannan PI-88. *Eur. J. Med. Chem.*, 37:783-791.

Figure Legends

Figure 1. Revised structure for PI-88 (**1**), and structures of the oligosaccharides from PI-88 and its non-sulfated precursor (**2**-**17**).

Figure 2. Superimposed HSQC spectra of sulfated (**7**) and non-sulfated (**6**) pentasaccharide fraction, showing significant chemical shift differences.

Figure 3: Decomposition of PI-88. The peaks indicated by the dotted lines differ significantly between the two samples. The bottom trace corresponds to the sample measured in Australia while the intermediate and lower traces correspond to the sample measured in Italy immediately after NMR tube preparation and after two days, respectively.

Figure 4. Glycosidic linkage ϕ/ψ Ramachandran plots of polysulfated pentasaccharide **7** (left column), and non-sulfated pentasaccharide **6** (right column), sampled in the last step of the MD simulation procedure (see Materials and Methods). The glycosidic linkages are indicated by the pairs of residues connected in going from the nonreducing (E) to the reducing end (A). The density colour maps qualitatively indicate the population of states ϕ/ψ that increase in going from blue to red colour, allowing the determination of the preferred conformations reported in Table 3. The corrected dihedral angles ϕ/ψ matching the inter-glycosidic H1-H3 and H5-H2 distances reported in Table 2, are shown in Table 3.

Figure 5. Polysulfated phosphomannopentaose **7** (right) and the corresponding non-sulfated precursor **6** (left), structures and conformations. The inter-glycosidic distances matching the corresponding restraints are reported in Table 2. The Man-α residue labels are reported from the non-reducing to the reducing end (E to A).

Table I. ^{1}H and ^{13}C NMR chemical shift data for PI-88 (**1**) at 600 MHz in D_2O

Residue		**H-1/C-1**	**H-2/C-2**	**H-3/C-3**	**H-4/C-4**	**H-5/C-5**	**H-6a,b/C-6**
α-Man-6-PO_4	E	5.53	5.30	4.91	4.84	4.33	4.22/4.18
		102.4	77.9	77.0	74.9	73.5	64.8
→3)-α-Man	D	5.51	5.06	4.43	4.72	4.39	4.61/4.44
		102.7	78.9	78.1	75.5	72.0	68.8
→3)-α-Man	C	5.52	5.10	4.42	4.67	4.43	4.43
		103.1	79.1	78.5	75.2	72.1	68.9
→3)-α-Man	B	5.59	4.87	4.39	4.58	4.17	4.40
		101.2	79.2	79.8	75.0	72.5	69.3
→2)-α-Man-OSO_3Na	A	5.845	4.56	4.83	4.67	4.30	4.55/4.28
		98.9	75.2/77.7	77.5	75.2/74.4	74.2	69.7
→2)-β-Man-OSO_3Na	A	5.63	4.69	4.78	?	4.11	4.60/4.23
		98.2	75.1	79.2	?	76.9	70.3
→2)-α-Man-OH	A	5.42	4.44	4.83			
		94.9	75.5				
→3)-α-Man-(1→2)-α-Man-OH	B	5.56					
		101.3					
→2)-β-Man-OSO_3Na	A	5.63	4.68	4.78	nd	4.10	
		98.2	75.3-75.7	79,2	nd	76.9	
→3)-α-Man-(1→2)-β-Man-OSO_3Na	B	5.71	4.89				
		100.4	79.3				

Table II. Intra- and inter-residue (bold) H-H distances of compound **7**, estimated by the spin pair approximation using NOE% at the lowest available mixing time (second column). The third colums include the H-H distances measured from compound **7** model setting the glycosidic angles ϕ/ψ, as estimated in the final (11^{th}) of the multi-step MD simultation procedure using the 2D histogram binning approach (see Materials and Methods).

Atom pair	Experimental distance (Å)	MD simulation 2D histogram bins (Å)
E1-D3	**2.2**	**2.3**
E2-E1	2.6	2.5
E2-E3	2.8	2.5
D1-C3	**2.3**	**2.2**
D2-E5	**2.5**	**2.9**
D2-D1	2.4	2.5
D2-D3	2.5	2.4
C1-B3	**2.4**	**2.2**
C2-D5	**2.5**	**3.1**
C2-C1	2.4	2.5
C2-C3	2.5	2.4
B1-A1	**3.4**	**3.0**
B2-C5	**2.5**	**2.8**
B1-A2	**2.4**	**2.2**
B2-B1	2.7	2.5
A1-B5	**3.0**	**3.0**
A1-B1	**2.8**	**3.0**

Table III. Glycosidic dihedral angle pairs ϕ/ψ as determined from the density colour map reported in Fig. 4

	ϕ/ψ Dihedral angles (°)	
Glycosidic linkage	**Sulfated pentasaccharide 7**	**Pentasaccharide 6**
E-D	-30/30	-30/50, -40/20, -40/-20 [a]
D-C	-30/40	-50/-10
C-B	-40/30	-40/-20
B-A	-30/40	-40/50

[a] The wide yellow/red area of ϕ/ψ Ramachandran plot obtained after the 2D histogram binning in pentasaccharide **6**, were graphically decomposed in three states, considering the continuity of the color map in Fig. 4 E-D panel right column.

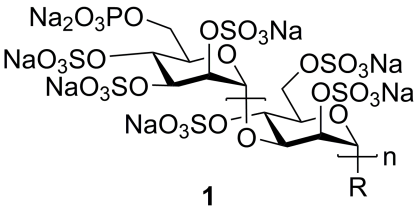

1

where R =
n = 0-3

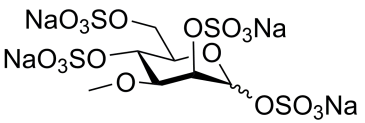

or

where R =
n =1-4

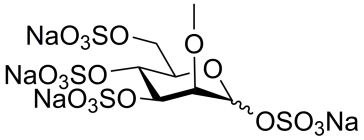

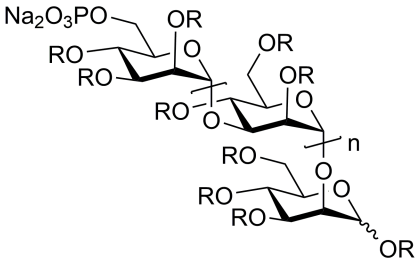

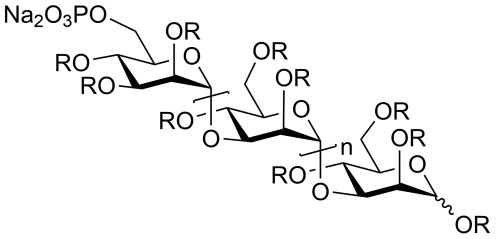

	n	R		n	R
2	1	H	**10**	0	H
3	1	SO_3Na	**11**	0	SO_3Na
4	2	H	**12**	1	H
5	2	SO_3Na	**13**	1	SO_3Na
6	3	H	**14**	2	H
7	3	SO_3Na	**15**	2	SO_3Na
8	4	H	**16**	3	H
9	4	SO_3Na	**17**	3	SO_3Na

Man6P-1,3-Man-1,3-Man-1,3-Man-1,2-Man

E D C B A

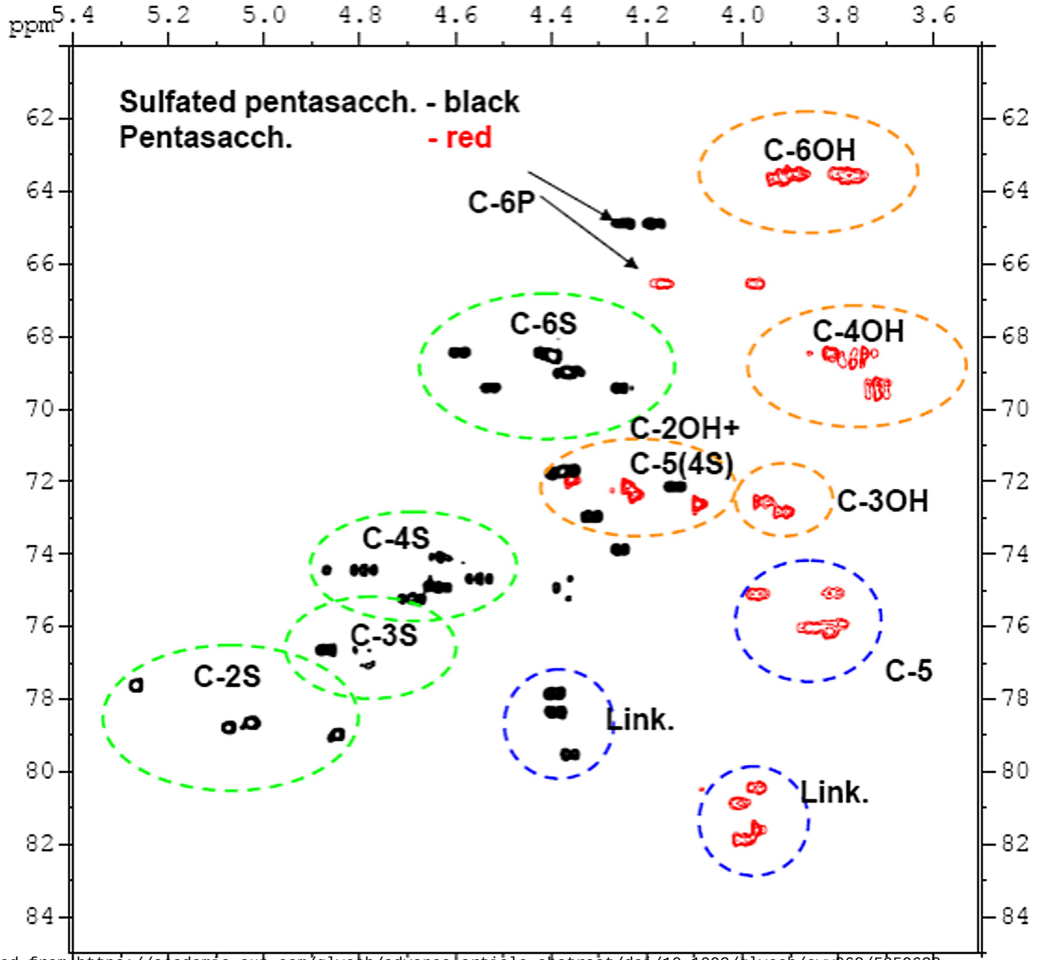

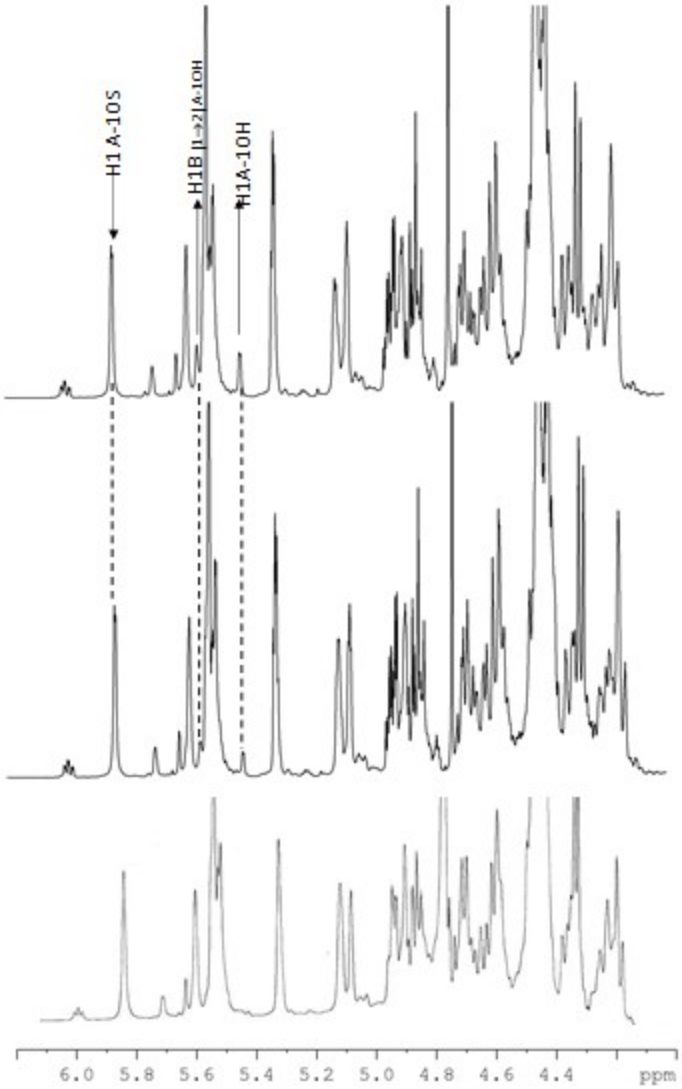

Poly-sulfated Phosphomannan Pentasaccharide

Not-sulfated Phosphomannan Pentasaccharide